batteries

MDPI

Article

Functional Surface Coating to Enhance the Stability of $LiNi_{0.6}Mn_{0.2}Co_{0.2}O_2$

Yingying Xie [1], Matthew Li [1], Jiantao Li [1], Xiaozhou Huang [1], Jiyu Cai [1], Zhenzhen Yang [1], Hoai Nguyen [1], Baasit ali Shaik sulaiman [2], Niloofar Karami [2], Natalya A. Chernova [2], Shailesh Upreti [2], Brad Prevel [2], Feng Wang [3] and Zonghai Chen [1,*]

[1] Chemical Sciences and Engineering Division, Argonne National Laboratory, 9700 Cass Ave., Lemont, IL 60439, USA; yxie@anl.gov (Y.X.); jiantao.li@anl.gov (J.L.); xiaozhou.huang@anl.gov (X.H.); jcai@anl.gov (J.C.); yangzhzh@anl.gov (Z.Y.); nguyenh@anl.gov (H.N.)

[2] Charge CCCV (C4V), Center of Excellence, Binghamton University, 45 Murray Hill Road, Vestal, NY 13850, USA; b.shaiksulaiman@c4v.us (B.a.S.s.); n.karami@c4v.us (N.K.); n.chernova@c4v.us (N.A.C.); s.upreti@c4v.us (S.U.); b.prevel@c4v.us (B.P.)

[3] Advanced Materials Division, Argonne National Laboratory, 9700 Cass Ave., Lemont, IL 60439, USA; fengwang@anl.gov

* Correspondence: zonghai.chen@anl.gov

Abstract: Parasitic reactions are responsible for continuous performance loss during the normal operation and storage of lithium-ion batteries, particularly for those using nickel-rich cathode materials. Among many contributors, residual Li_2CO_3 on the surface of nickel-rich cathodes plays a detrimental role in promoting parasitic reactions, and hence accelerates the performance loss of those cathode materials. In this work, a wet impregnation process was utilized to convert the detrimental Li_2CO_3 and LiOH impurities into a beneficial functional surface coating comprising phosphates. Specifically, hydro-phosphates were used as the functional surface modification agents to mitigate the detrimental effect of surface residuals. The best electrochemical performance was achieved by modifying $LiNi_{0.6}Mn_{0.2}Co_{0.2}O_2$ with a diluted dihydro-phosphate solution (pKa = 7.2), while the metal cation had a negligible impact on the electrochemical performance. This work provides a cheap and simple method for enabling the high performance of nickel-rich cathodes.

Keywords: nickel-rich cathode; Li_2CO_3; parasitic reaction; surface modification; wet impregnation

check for updates

Citation: Xie, Y.; Li, M.; Li, J.; Huang, X.; Cai, J.; Yang, Z.; Nguyen, H.; Shaik sulaiman, B.a.; Karami, N.; Chernova, N.A.; et al. Functional Surface Coating to Enhance the Stability of $LiNi_{0.6}Mn_{0.2}Co_{0.2}O_2$. *Batteries* **2023**, *9*, 485. https://doi.org/10.3390/batteries9100485

Academic Editor: A. Robert Armstrong

Received: 24 August 2023
Revised: 9 September 2023
Accepted: 20 September 2023
Published: 23 September 2023

1. Introduction

Nickel-rich lithium transition metal oxides can operate at a relatively high potential and deliver a high reversible specific capacity up to 220 mAh g^{-1}. Therefore, they are widely regarded as promising cathode materials for high-energy-density lithium-ion technologies. Unlocking their potential for a higher energy density does come with additional barriers to overcome [1]. These include insufficient structural and interfacial stability that simply cannot support their long-term operation [2–5]. Many structural and morphological changes have been widely reported regarding extensively cycled nickel-rich cathodes. These observations include detrimental H1-3/O1 phase transformation at a high potential [6,7], dissolution and migration of the transition metal from the cathode to the anode [8–10], surface reconstruction (a process resulting in the formation of spinel-like and rock salt structure on the surface of cathode particles) [11–14], and the microcracking between primary particles [15–18] and within single primary particles [19]. Most of these observations are based on the bulk properties of the lithium transition metal oxides, and interestingly, a lot of these observations were reported to be overcome by surface-focused approaches like surface coating and surface doping [3,4,18,20,21]. Using in situ high-energy X-ray diffraction (HEXRD) to track the structural evolution of lithium nickel–manganese–cobalt oxides (NMC) during charge/discharge cycling, Xu et al. reported that NMC slowly

underwent undesired phase transformation from the layered structure to a spinel-like structure when cycled to a high potential, and that this undesired phase transformation can be successfully eliminated by a thin layer of poly(3,4-ethylenedioxythiophene) (PEDOT) coating on the surface of NMC secondary particles [14]. Using electron microscopy to track the morphological change in NMC cathodes, Zhang et al. observed the formation of microcracks inside NMC particles after extensive cycling. They also reported that the cracking issue can be resolved by applying a thin layer of Li_3PO_4 coating on the NMC surface [17]. Independently, Chen et al. reported that the microcracks can also be overcome by applying a layer of elastic PEDOT coating [18]. Dahn et al. reported that, when charged to 4.5 V vs. Li^+/Li, $LiCoO_2$ underwent an irreversible phase transformation from H1-3 phase to O1 phase, physically achieved through the gliding of adjacent CoO_6 octahedron layers on the ab plane [6], triggering the accelerated electrochemical performance loss of $LiCoO_2$. They also reported that this phase transformation can become reversible when the $LiCoO_2$ particle is coated with Al_2O_3 [6]. Hu et al. also reported that the stable cycling of NMC up to 4.8 V vs. Li^+/Li can be accomplished by deploying a functional electrolyte additive to stabilize the cathode/electrolyte interface (CEI) [7]. Clearly, the change in surface chemistry can have a significant impact on the bulk mechanical/crystallographic behavior of NMC cathode materials. However, a consensus on the physical connection between the surface chemistry and the bulk properties has not been reached yet.

Due to the urgent need to understand the surface chemistry of NMC cathodes, a major effort has been devoted to characterizing the chemical composition of CEI, as well as their 3D distribution, using cutting-edge characterization tools [22–25], in attempts to identify the fingerprint of a good CEI. With the continuous evolution of new concepts and new characterization capacities, the chemical and physical image of a good CEI is continuously updating, but a consensus on universally good CEI has not been achieved yet. On the other hand, there is an emerging effort to quantitatively measure the electrochemical functionality of the CEI layer, to block the electron transfer between the electrolyte and the electrode materials, using advanced electrochemical characterization such as high precision columbic efficiency (HPCE) [26,27] and high-precision leakage current (HpLC) [28–31] measurements. Both HPCE and HpLC results show that, even with the presence of the best SEI or CEI, there are persistent parasitic reactions ongoing inside lithium-ion cells. The parasitic reactions are a set of chemical/electrochemical reactions between the electrolyte and the electrode material that cause the continuous loss of electrochemical performance of the lithium-ion cell. It was recently reported that an important step of the parasitic reactions on the cathode side is the chemical oxidation reaction of the carbonate solvents with the help from the exposed transition metal cations on the cathode surface [29]. Meanwhile, residual Li_2CO_3 is generally found on the surface of nickel-rich cathode materials. It was also reported that residual Li_2CO_3 can promote the chemical absorption of carbonate solvents, and hence promote the electron transfer reaction between the electrolyte and the delithiated cathodes [32]. Therefore, the presence of residual Li_2CO_3 plays a detrimental role in accelerating the parasitic reactions, increasing the CO_2 generated at high potentials [33,34], aggravating the surface reconstruction, and accelerating the performance loss of nickel-rich cathodes [32]. Therefore, mitigating the impact of exposed transition metal cations and residual Li_2CO_3 is crucial for maintaining the high performance of nickel-rich cathodes.

In this work, we aim to mitigate the detrimental impact of exposed transition metal cations and residual Li_2CO_3 on $LiNi_{0.6}Mn_{0.2}Co_{0.2}O_2$ (NMC622) through a simple one-step surface modification. By adopting a wet impregnation process, hydro-phosphates were used as the chemical reaction agent to remove residual $LiOH/Li_2CO_3$, and at the same time, deposit a thin layer of phosphates on the cathode surface as the functional coating material. It was demonstrated that phosphate coating is beneficial for improving the electrochemical performance of NMC622, and weak acids like dihydro-phosphates (pKa = 7.2) give the best protection to NMC622.

2. Materials and Methods

Absorbing capacity measurement—First, 10 g of NMC622 powder was fully soaked in 30 mL of water. The wet powder was separated from the liquid and collected after centrifuging. The powder was then baked at 550 °C overnight to remove the absorbed water on the surface of NMC622. The difference in weight before and after baking was then used as the water absorption capability for NMC622. In this study, the average value was determined to be about 15 wt% of the NMC622 powder. For the wet impregnation process, a 20 wt% liquid was used to minimize the residual liquid on the NMC622 powder after wetting with the intended surface modification solutions.

LiOH/Li_2CO_3 Titration—First, 0.5 g NMC622 powder was soaked in 30 mL of deionized (DI) water for minutes to allow the dissolution of residual LiOH and Li_2CO_3 in the aqueous phase. The liquid was then separated from the wet NMC622 powder after centrifuging. Then, 2 mL of the obtained liquid phase was sampled for titration using a Mettler Toledo T5 Excellence automatic titrator. The titration solution used was a 0.01 M HCl solution. The titration curve was then used to calculate the content of residual LiOH and L_2CO_3 in the NMC622 powder.

Material processing—First, 10 g NMC622 was added to a plastic bottle, followed by 2 mL of surface modification solution with the appropriate amount of acid based on the designed ratios. For example, the sample NMC622-Ca-1 had a 2 mL surface modification solution with a 1 wt% of $Ca(H_2PO_4)_2$. The wet powder was then further mixed using Resodyn Acoustic Mixer for 2 min to ensure uniform coverage of the modification solution on theNMC622 surface. Subsequently, the wet NMC622 powder was then baked at 550 °C for 6 h, sufficient for the complete removal of moisture and to deposit phosphates on the surface of NMC622. The surface-modified samples were labeled as NMC622-SMA-x, where x is the weight percentage of the surface modification agent SMA in the liquid solution, and where Al stands for $Al(H_2PO_4)_3$, Ca stands for $Ca(H_2PO_4)_2$, Mg stands for $MgHPO_4$, H stands for H_3PO_4, and B stands for H_3BO_3.

Cell assembling and electrochemical characterization—The electrochemical performances of NMC22 cathodes with and without surface modification were characterized in 2032R coin-type cells, using lithium metal as the counter electrode. The active cathode material, conductive additive (Carbon 45), and binder (polyvinylidene–fluoride, PVDF) were suspended in N-methyl-2-pyrrolidone (NMP) with a mass ratio of 92:4:4 to form a slurry. The obtained slurry was applied to an Al current collector, dried, and then cut into 14 mm diameter disks with a cathode loading level of 9–10 mg cm^{-2}. The electrolyte consisting of 1.2 M LiPF6 in ethylene carbonate/ethyl methyl carbonate solution (EC:DMC = 3:7 by wt.) was used. The half-coin cells were assembled in an Ar-filled glove box. Each coin cell consisted of a cathode electrode and a Li chip anode electrode with a layer of separator in between. Galvanostatic cycle tests were performed on a LAND system in a voltage range from 2.5 to 4.4 V (vs Li^+/Li), with a constant current of C/3.

XPS characterization—Surface coating analysis on the NMC particles was carried out using X-ray photoelectron spectroscopy (XPS) in a PHI 5000 VersaProbe II system manufactured by Physical Electronics. The instrument was connected to an argon glovebox to ensure a controlled atmosphere during the analysis. The XPS spectrometer utilized a focused monochromatic radiation beam with a diameter of 100 μm and a power output of 25 W. The radiation source employed was Al Kα with an energy of 1486.6 electron volts (eV). High-resolution spectra were obtained using electron beam sample neutralization, fixed analyzer transmission mode, and a constant pass energy of 23.25 eV. The analyzed area of the samples measured 100 × 100 μm^2 in dimensions. The binding energy calibration was performed using the hydrocarbon (C-C) peak in the C 1s spectrum, which was set at 284.8 eV.

3. Results

3.1. Surface Modification of NMC622

Figure 1 schematically shows the wet impregnation process to remove residual $LiOH/Li_2CO_3$ and deposit a functional coating material on the surface of NMC622. Instead of fully soaking the NMC622 powder in an excessive amount of liquid solution, the NMC622 powder was initially mixed with a limited amount of solution (20 wt% of NMC622 powder), containing a surface modification agent like $Ca(H_2PO_4)_2$, followed by acoustic mixing to uniformly disperse the solution on the surface of the NMC622 powder. After mixing, the wet power was then baked at 550 °C for 6 h to remove moisture and deposit phosphates on the NMC622 surface (see Equations (1) and (2) for exemplary reactions).

$$12LiOH + 3Ca(H_2PO_4)_2 \rightarrow 4Li_3PO_4 + Ca_3(PO_4)_2 + 12H_2O \quad (1)$$

$$6Li_2CO_3 + 3Ca(H_2PO_4)_2 \rightarrow 4Li_3PO_4 + Ca_3(PO_4)_2 + 6H_2O + 6CO_2 \quad (2)$$

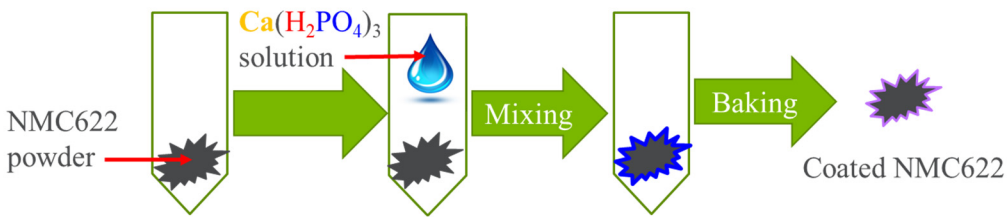

Figure 1. Schematics of wet impregnation for depositing functional surface coating on NMC622 ($LiNi_{0.6}Mn_{0.2}Ni_{0.2}O_2$).

Before conducting the surface modification, NMC622 was first fully soaked with deionized water. After being separated from the liquid phase, the wet powder was baked at 550 °C overnight. About 15 wt% weight loss was observed during the thermal processing, suggesting at least 15 wt% water is needed to saturate the surface area of NMC622. In the real process, the amount of liquid was set at 20 wt% to ensure full adsorption with a limited amount of excessive liquid. Meanwhile, a titration procedure was used to determine the content of residual LiOH and Li_2CO_3 on the surface of NMC622 (see Figure 2 for the titration curves). The titration results indicate that the content of LiOH and Li_2CO_3 is 1900 and 4500 ppm (0.19 wt% and 0.45 wt%) of NMC622 powder, respectively. Based on the content of the residual $LiOH/Li_2CO_3$, one can calculate the targeted concentration of various hydro-phosphates that can provide the proper number of protons to neutralize the residual LiOH and Li_2CO_3 as summarized in Table 1. The sample ID, processing condition, and basic electrochemical properties of surface-modified NMC622 are outlined in Table 2 for a direct comparison.

Table 1. Targeted concentration for different surface modification agents for complete removal of residual $LiOH/Li_2CO_3$ in NMC622.

Surface Modification Agent	Targeted Concentration
$Ca(H_2PO_4)_2 \cdot H_2O$	6.5 wt%
$Al(H_2PO_4)_3$	5.0 wt%
$MgHPO_4 \cdot 3H_2O$	17.5 wt%
H_3PO_4	3.3 wt%

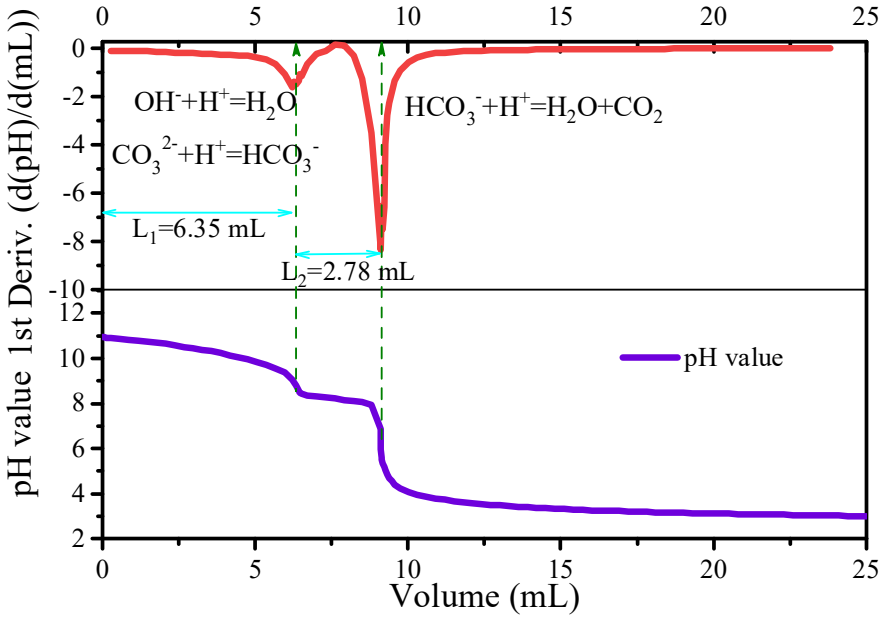

Figure 2. Titration curve to determine the level residual $LiOH/Li_2CO_3$ in $LiNi_{0.6}Mn_{0.2}Co_{0.2}O_2$.

Table 2. Basic electrochemical properties of NMC622 processed with different surface modification solutions.

Sample ID	Processing Solution	1st Charge Capacity (mAh g^{-1})	1st Discharge Capacity (mAh g^{-1})	1st Cycle Columbic Efficiency, %	Capacity Retention @ 50th Cycle, %
NMC622		205.0 ± 1.84	182.2 ± 2.40	89.04 ± 0.35	92.08 ± 1.59
NMC622-Ca-1	1 wt% $Ca(H_2PO_4)_2$	207.9 ± 2.25	181.1 ± 1.94	87.10 ±0.08	96.21 ± 0.28
NMC622-Ca-3	3 wt% $Ca(H_2PO_4)_2$	209.5 ± 2.04	180.7 ± 0.64	86.23 ± 0.53	97.25 ± 0.87
NMC622-Ca-4	4 wt% $Ca(H_2PO_4)_2$	202.8 ± 0.85	175.7 ± 1.13	86.65 ± 0.21	95.48 ± 0.25
NMC622-Al-p5	0.5 wt% $Al(H_2PO_4)_3$	207.6 ± 1.91	184.2 ± 1.34	88.73 ± 0.16	94.09 ± 1.17
NMC622-Al-1	1 wt% $Al(H_2PO_4)_3$	211.3 ± 1.97	187.4 ± 1.33	88.73 ± 0.05	94.49 ± 0.45
NMC622-Al-2	2 wt% $Al(H_2PO_4)_3$	209.4 ± 1.94	180.2 ± 0.40	86.06 ± 0.01	96.53 ± 0.03
NMC622-Al-3	3 wt% $Al(H_2PO_4)_3$	208.8 ± 0.78	180.2 ± 0.42	86.32 ± 0.12	97.56 ± 0.73
NMC622-Mg-5	5 wt% $MgHPO_4$	207.9 ± 1.01	183.7 ± 0.95	88.33 ± 0.05	93.42 ± 0.81
NMC622-Mg-10	10 wt% $MgHPO_4$	203.4 ± 0.92	179.3 ± 0.45	88.33 ± 0.06	89.01 ± 3.26
NMC622-Mg-15	15 wt% $MgHPO_4$	196.1 ± 2.82	173.2 ± 1.70	88.32 ± 0.03	89.77 ± 0.95
NMC622-H-1	1 wt% H_3PO_4	199.9±1.22	177.0± 1.23	88.53± 0.21	94.50± 0.67
NMC622-H-3	3 wt% H_3PO_4	205.9±0.90	184.5± 0.85	89.96± 0.07	94.50± 0.67

3.2. Surface Chemistry of NMC622

To confirm the effectiveness of the surface modification on NMC622, X-ray photoelectron spectroscopy (XPS) was deployed to characterize the change in surface chemistry as shown in Figure 3. The first column of Figure 3 presents the high-resolution spectra of the *Ca2p* core level for the pristine NMC622, and those modified with the $Ca(H_2PO_4)_2$ solution. No *Ca2p* signal was observed for the pristine NMC622 powder as expected, and those samples modified with $Ca(H_2PO_4)_2$ solutions clearly show strong absorption at a binding energy of 350.3 eV ($Ca2p_{1/2}$) and 346.8 eV ($Ca2p_{3/2}$), respectively. This clearly illustrates the deposition of Ca-bearing species through the wet impregnation process. The high-resolution *P2p* spectra also clearly show the deposition of phosphate-bearing species on the modified NMC622 particles, evidenced by the characteristic absorption peak at a binding energy of 133.7 eV (see the second column of Figure 3). It is one of our main objectives to mitigate the catalytic impact of residual Li_2CO_3. Therefore, the high-resolution spectra of *C1s* were also collected and are shown in the third column of Figure 3. It can be clearly seen that the *C1s* absorption peak at a 289.7 eV binding energy decreases quickly

with the increase in $Ca(H_2PO_4)_2$ in the processing solution. The decrease in *C1s* signal can come from two possible roots, either Li_2CO_3 being buried under a thicker coating layer or more Li_2CO_3 being removed by the processing solution. To differentiate between possible roots, high-resolution *Ni2p* spectra were also collected (see the last column of Figure 3) and used as the internal reference for *C1s* spectra, considering the Ni element to be covered with the same surface coating layer as Li_2CO_3. Therefore, the intensity ratio between the *C1s* peak at 289.7 eV and the $Ni2p_{3/2}$ peak at 854.7 eV can be used as a quantitative indicator for the level of residual Li_2CO_3. It was found that the peak ratio decreased from 0.129 (NMC622) to 0.06 (NMC622-Ca-1), 0.05 (NMC622-Ca-3), and 0.05 (NMC622-Ca-4), respectively. Clearly, the majority of residual Li_2CO_3 was removed with a low $Ca(H_2PO_4)_2$ concentration level up to 1 wt%, and the effectiveness of Li_2CO_3 removal slows down with a further increase in the concentration of $Ca(H_2PO_4)_2$. The reduced effectiveness can be attributed to the very low Ksp of $Ca_3(PO4)_2$ (1.08×10^{-23}), which can be translated into a very low solubility (~10–5 M, or ~3 ppm) in neutral water. When $Ca(H_2PO_4)_2$ comes into contact with a residual Li_2CO_3 domain, $Ca_3(PO_4)_2$ quickly forms and in situ deposits on top of the Li_2CO_3 domain, passivating the Li_2CO_3 surface and slowing down the removal of Li_2CO_3.

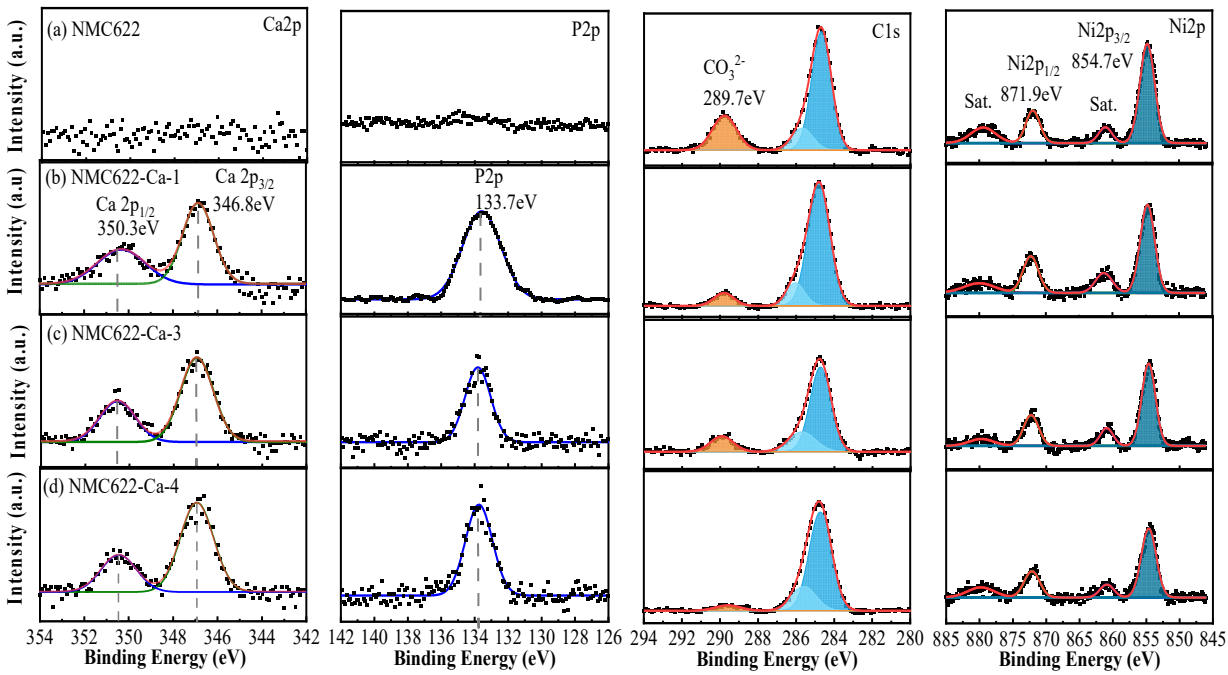

Figure 3. XPS results showing the deposition of phosphates on the surface of (**a**) pristine NMC622; (**b**) NMC622-Ca-1; (**c**) NMC622Ca-3; and (**d**) NMC622-Ca-4. Dotted lines represent raw spectrum and solid lines represent fitted spectrum. Some peak areas were colored to guide reader.

3.3. Electrochemical Performance of NMC622

Figure 4a shows the normalized capacity retention of half cells using pristine NMC622, and those modified with different concentrations of $Ca(H_2PO_4)_2$ solutions. The corresponding voltage profile and dQdV of NMC622 and NMC622-Ca-3 are shown in Figure 4b,c and Figure 4d,e, respectively. The electrolyte used for these cells is 1.2 M LiPF6 in a mixture solvent of ethylene carbonate (EC) and ethyl methyl carbonate (EMC) with a mass ratio of 3:7. Before continuously cycling between 2.5 V and 4.4 V vs. Li^+/Li using a constant current of C/3 (~1.0 mA), these cells were first subject to two formation cycles between 2.5 V and 4.4 V at a constant current of C/10. From the voltage profiles and dQdV, it was apparent that the coating layer offered more stable cycling with lower impedance at high cycle numbers. The basic electrochemical performance of these cells is summarized in Table 2. The first discharge capacity obtained from the formation cycles was used as the initial discharge

capacity to normalize the discharge capacity retention as shown in Figure 4. As shown in Table 2, the initial specific discharge capacity decreases steadily with the concentration of $Ca(H_2PO_4)_2$, implying that more inactive phosphate material was deposited. Although we initially expected that the final phosphate-based coating material could protect NMC622 from reaction with the electrolyte during repeating charge/discharge cycling [15,35], it was observed that the first cycle columbic efficiency of NMC622 cathodes slightly decreases with the concentration of $Ca(H_2PO_4)_2$, which is quite different from the capacity retention shown in Figure 4. It is speculated here that, with a very low solubility of $Ca_3(PO_4)_2$, the residual Li_2CO_3 was effectively passivated by $Ca_3(PO_4)_2$, and the rest of $Ca(H_2PO_4)_2$ alternatively attacked the NMC622 surface that was not covered by Li_2CO_3, causing a slight degradation on the surface of NMC622. Therefore, a lower concentration of $Ca(H_2PO_4)_2$ is preferred to leave a lower amount of excessive $Ca(H_2PO_4)_2$ to attack active NMC622 material. This also reflects the cycling results shown in Figure 4, that NMC622 modified with a low $Ca(H_2PO_4)_2$ concentration of 3 wt%, which is far below the targeted concentration as shown in Table 1, had the best capacity retention. On the other hand, the 1 wt% sample did not perform as well as the 3 wt%, likely because the Li_2CO_3 surface was not sufficiently passivated by such a low amount of weak acid, and it still retained its cycle degrading function. This interplay between passivating the surface of Li_2CO_3 and not having too great an excess number of protons that can attack the NMC622 is the likely reason for the existence of an optimal point (3 wt%).

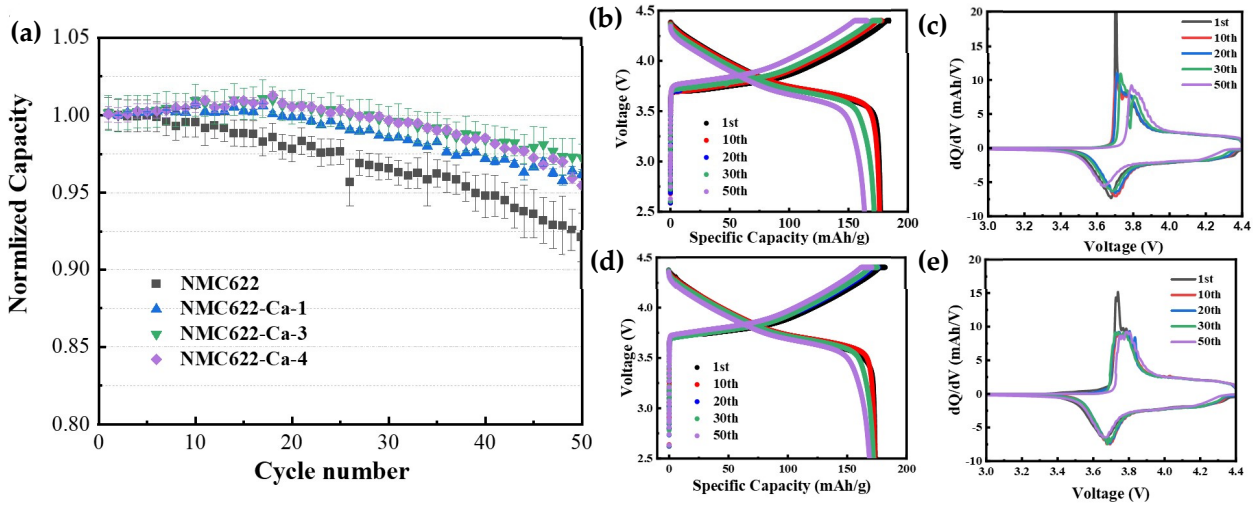

Figure 4. (**a**) Discharge capacity of half cells during charge/discharge cycling between 2.5 V and 4.4 V with a constant current of C/3 (~1 mA), showing the impact of $Li_3PO_4/Ca_3(PO_4)_2$ coating on the performance of NMC622. (**b**) Voltage profile of NMC622 and (**c**) corresponding dQdV. (**d**) Voltage profile of NMC622-Ca-3 and (**e**) corresponding dQdV. Please note the 1st cycle is taken after formation cycles.

4. Discussion

To generalize our observations, the same wet impregnation process was deployed to treat the NMC622 cathode with various hydro-phosphate solutions including $Al(H_2PO_4)_3$, $Mg(H_2PO_4)_2$, and H_3PO_4, and the electrochemical results are compared in Table 2. With different surface modification agents, the same trend was maintained; that is, both the initial irreversible capacity loss and the reversible specific capacity decrease with the concentration of the surface modification agent. When it comes to the capacity retention, the best hydro-phosphate concentration was found to be 3 wt% for H_3PO_4, 3 wt% for $Ca(H_2PO_4)_2$, 3 wt% for $Al(H_2PO_4)_3$, and 5 wt% for $MgHPO_4$. Figure 5 compared the normalized capacity retention of the best materials from each class. The pristine MNC622 lost about 8% of its reversible capacity after 50 cycles. Compared to pristine NMC622, NMC622-H-3 and MNC622-Mg-5 had a slightly better capacity retention, losing about 6% of

their reversible capacity after 50 cycles. The best electrochemical performance was observed for those modified with either $Ca(H_2PO_4)_2$ or $Al(H_2PO_4)_3$, while no significant difference was observed between them. This suggests that the anion, PO_4^{3-}, plays an active role in protecting the NMC622 cathode from reacting with the electrolyte during the continuous charge/discharge cycling, and to maintain a better capacity retention. Considering the need to mitigate the detrimental impact of residual Li_2CO_3, the pH value of the processing solution should also play an active role in the electrochemical performance. In an aqueous solution, H_3PO_4 behaves as a triprotic acid, as shown in Equations (3)–(5).

$$H_3PO_4 \rightleftharpoons H_2PO_4^- + H^+, \qquad pKa1 = 2.14 \tag{3}$$

$$H_2PO_4^- \rightleftharpoons HPO_4^{2-} + H^+, \qquad pKa2 = 7.20 \tag{4}$$

$$HPO_4^{2-} \rightleftharpoons PO_4^{3-} + H^+, \qquad pKa3 = 12.37 \tag{5}$$

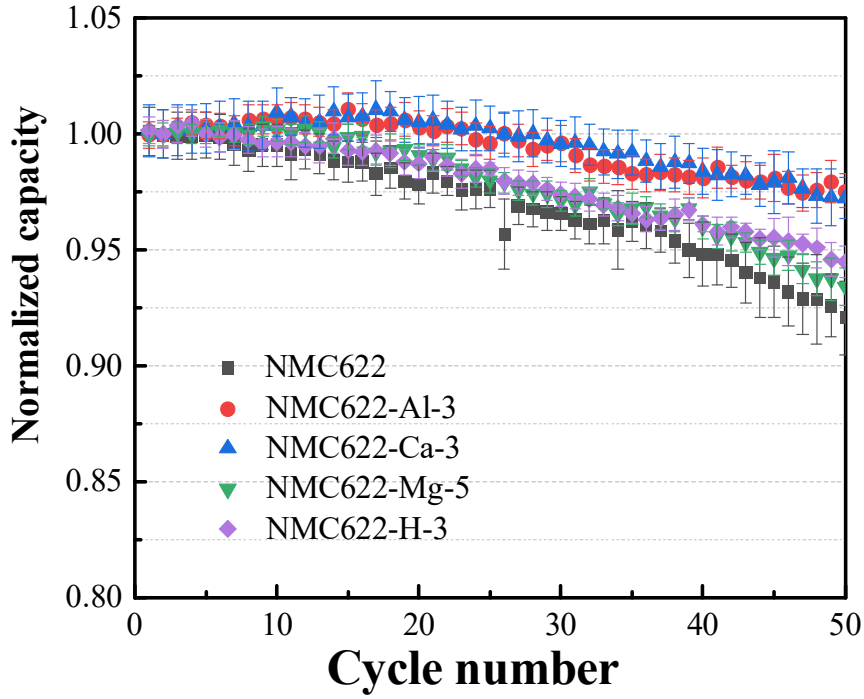

Figure 5. Comparison of the capacity retention of NMC622 processed with different acidic phosphate-based solutions.

Among all surface modification agents examined, the H_3PO_4 solution had the lowest pH (pKa1 = 2.14), and NMC622 particles were expected to get more aggressively attacked by the excessive H_3PO_4 solution that is absorbed on the bare NMC622 surface, and hence less improvement in capacity retention was observed. On the other hand, $MgHPO_4$ is a weak acid (pKa3 = 12.37), and it has very limited capacity to neutralize the residual Li_2CO_3. To validate the importance of the PO_4^{3-} anion and the pH of the processing solution, different concentrations of H_3BO_3 were deployed to the treated NMC622 material using the same wet impregnation process. As shown in Figure 6, no significant difference was observed among NMC622 samples with and without the H_3BO_3 treatment. The ineffectiveness can be ascribed to (1) a high pKa1 (9.2, a weak acid) and (2) the lack of PO_4^{3-} that is desired to protect NMC622. Therefore, one can conclude that weak acids comprising dihydro-phosphates are ideal candidates to serve the purpose of both passivating residual Li_2CO_3 and depositing a functional surface coating layer with minimum damage to the NMC622 material.

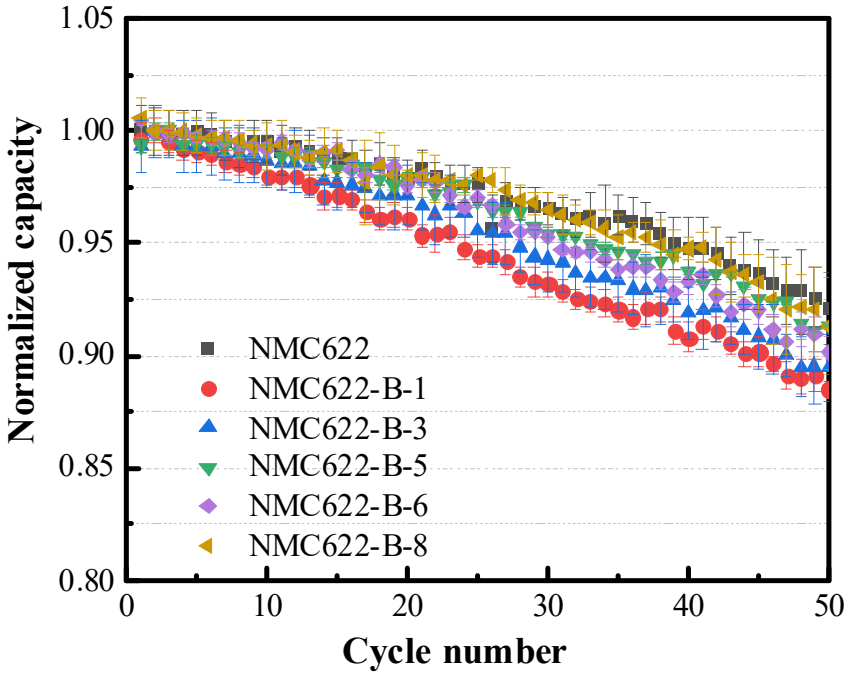

Figure 6. Discharge capacity of half cells during charge/discharge cycling between 2.5 V and 4.4 V with a constant current of C/3 for $LiNi_{0.6}Mn_{0.2}Co_{0.2}O_2$ with and without modification with H_3BO_3. The concentration of H_3BO_3 in the solution is 1 wt% (NMC622-B-1), 3 wt% (NMC622-B-3), 5 wt% (NMC622-B-5), 6 wt% (NMC622-B-6), and 8 wt% (NMC622-B-8), respectively.

Summarizing the above discussion, Figure 7 schematically illustrates the working mechanism of the phosphate-based functional surface coating to improve the electrochemical performance of NMC622. On the surface of pristine NMC622 particles, there are exposed transition metal cations that are not fully encapsulated in TMO_6 octahedrons. The partially empty d orbitals of these exposed transition metal cations are good electron acceptors while the carbonyl group of carbonate solvent serves well as a good electron donor. When NMC622 particles come into contact with carbonate-based non-aqueous electrolytes, a coordination bond can be formed between the exposed transition metal cations and carbonate solvent, promoting the chemical absorption of solvent molecules on the NMC622 surface [29]. At the same time, the NMC622 surface can also be partially covered by residual Li_2CO_3, which is formed during the cooling-of-synthesis process, as well as storage at ambient conditions. Owing to the structural similarity between CO_3^{2-} units in the inorganic crystal and the carboxyl group in carbonate molecules, alkali carbonates have been widely used as the catalyst for the synthesis of organic carbonates by taking advantage of suitable chemical adsorption energy for organic carbonates on the surface of inorganic carbonates [36,37]. In the case of NMC622, the residual Li_2CO_3 can also promote the chemical adsorption of carbonate solvents via the Li_2CO_3 surface. In both cases, the chemically adsorbed carbonate molecules are prone to losing one electron to the NMC622 cathode material and undergoing a ring-opening reaction when it is charged to a relatively high potential—say, 4.2 V vs. Li^+/Li and above—leading to accelerated parasitic reactions and the electrochemical performance loss of NMC622. When the pristine NMC622 material is processed with the proposed hydro-phosphate solutions, a thin layer of metal phosphate will uniformly cover the surface of NMC622, as well as residual Li_2CO_3. This layer of phosphate acts as the physical barrier to block the chemical bonding between the NMC622 particle and the carbonate solvents, and hence the parasitic reactions on CEI can be effectively suppressed, leading to extended cycle life for the NMC622 cathode.

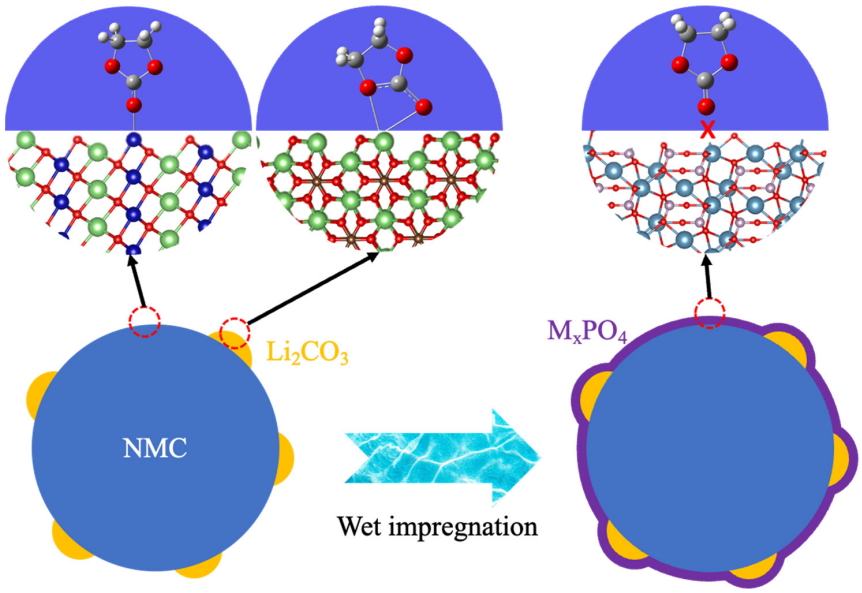

Figure 7. Schematics illustrates the mechanism for stabilized cathode/electrolyte interface with the functional surface coating.

5. Conclusions

A wet impregnation process is adopted to convert the detrimental Li_2CO_3 residual to a uniform thin layer of phosphate coating material on the surface of NMC622 particles. Although the residual Li_2CO_3 is only partially removed by the wet impregnation process, the low solubility of metal phosphates promotes the formation of uniform thin coating on the NMC622 particles, including the surface for residual Li_2CO_3. This functional coating layer can effectively block the specific chemical interaction between the carbonate solvent molecules and the NMC622 particles, demote the parasitic reactions, and ultimately improve the CEI stability of the NMC622 cathode. The comparison among various surface coating agents also reveals that a weak acid like dihydro-phosphate is highly desired to achieve the maximum protection with a minimum adverse impact on the nickel-rich cathode materials.

Author Contributions: Conceptualization, Z.C.; methodology, Y.X. and Z.Y.; validation, J.L., J.C., X.H., H.N., B.a.S.s., N.K., N.A.C., S.U., B.P. and F.W.; formal analysis Y.X., M.L. and Z.Y.; writing—original draft preparation, Z.C.; writing—review and editing, all authors; visualization, Y.X. and Z.C.; supervision, Z.C. All authors have read and agreed to the published version of the manuscript.

Funding: Research at Argonne National Laboratory was supported by the U.S. Department of Energy (DOE), Office of Energy Efficiency and Renewable Energy, Advanced Manufacturing Office. Argonne National Laboratory is operated for the DOE Office of Science by UChicago Argonne, LLC, under Contract DE-AC02-06CH11357.

Data Availability Statement: Not applicable.

Acknowledgments: Research at Argonne National Laboratory was supported by the U.S. Department of Energy (DOE), Office of Energy Efficiency and Renewable Energy, Advanced Manufacturing Office. Argonne National Laboratory is operated for the DOE Office of Science by UChicago Argonne, LLC, under Contract DE-AC02-06CH11357.

Conflicts of Interest: The authors declare no conflict of interest.

References

1. Sun, Y.-K.; Lee, D.-J.; Lee, Y.J.; Chen, Z.; Myung, S.-T. Cobalt-Free Nickel Rich Layered Oxide Cathodes for Lithium-Ion Batteries. *ACS Appl. Mater. Interfaces* **2013**, *5*, 11434–11440. [CrossRef]
2. Dose, W.M.; Temprano, I.; Allen, J.P.; Björklund, E.; O'Keefe, C.A.; Li, W.; Mehdi, B.L.; Weatherup, R.S.; De Volder, M.F.L.; Grey, C.P. Electrolyte Reactivity at the Charged Ni-Rich Cathode Interface and Degradation in Li-Ion Batteries. *ACS Appl. Mater. Interfaces* **2022**, *14*, 13206–13222. [CrossRef] [PubMed]
3. Li, G.; Feng, Y.; Zhu, J.; Mo, C.; Cai, Q.; Liao, Y.; Li, W. Achieving a Highly Stable Electrode/Electrolyte Interface for a Nickel-Rich Cathode via an Additive-Containing Gel Polymer Electrolyte. *ACS Appl. Mater. Interfaces* **2022**, *14*, 36656–36667. [CrossRef]
4. Wang, S.; Dai, A.; Cao, Y.; Yang, H.; Khalil, A.; Lu, J.; Li, H.; Ai, X. Enabling stable and high-rate cycling of a Ni-rich layered oxide cathode for lithium-ion batteries by modification with an artificial Li+-conducting cathode-electrolyte interphase. *J. Mater. Chem. A* **2021**, *9*, 11623–11631. [CrossRef]
5. Liu, T.; Yu, L.; Lu, J.; Zhou, T.; Huang, X.; Cai, Z.; Dai, A.; Gim, J.; Ren, Y.; Xiao, X.; et al. Rational design of mechanically robust Ni-rich cathode materials via concentration gradient strategy. *Nat. Commun.* **2021**, *12*, 6024. [CrossRef]
6. Chen, Z.; Lu, Z.; Dahn, J.R. Staging Phase Transitions in Lix CoO_2. *J. Electrochem. Soc.* **2002**, *149*, A1604. [CrossRef]
7. Tan, S.; Shadike, Z.; Li, J.; Wang, X.; Yang, Y.; Lin, R.; Cresce, A.; Hu, J.; Hunt, A.; Waluyo, I.; et al. Additive engineering for robust interphases to stabilize high-Ni layered structures at ultra-high voltage of 4.8 V. *Nat. Energy* **2022**, *7*, 484–494. [CrossRef]
8. Zhan, C.; Lu, J.; Jeremy Kropf, A.; Wu, T.; Jansen, A.N.; Sun, Y.-K.; Qiu, X.; Amine, K. Mn(II) deposition on anodes and its effects on capacity fade in spinel lithium manganate–carbon systems. *Nat. Commun.* **2013**, *4*, 2437. [CrossRef]
9. Jung, R.; Linsenmann, F.; Thomas, R.; Wandt, J.; Solchenbach, S.; Maglia, F.; Stinner, C.; Tromp, M.; Gasteiger, H.A. Nickel, Manganese, and Cobalt Dissolution from Ni-Rich NMC and Their Effects on NMC622-Graphite Cells. *J. Electrochem. Soc.* **2019**, *166*, A378. [CrossRef]
10. Wachs, S.J.; Behling, C.; Ranninger, J.; Möller, J.; Mayrhofer, K.J.J.; Berkes, B.B. Online Monitoring of Transition-Metal Dissolution from a High-Ni-Content Cathode Material. *ACS Appl. Mater. Interfaces* **2021**, *13*, 33075–33082. [CrossRef]
11. Xu, C.; Märker, K.; Lee, J.; Mahadevegowda, A.; Reeves, P.J.; Day, S.J.; Groh, M.F.; Emge, S.P.; Ducati, C.; Layla Mehdi, B.; et al. Bulk fatigue induced by surface reconstruction in layered Ni-rich cathodes for Li-ion batteries. *Nat. Mater.* **2021**, *20*, 84–92. [CrossRef] [PubMed]
12. Liu, X.; Hao, J.; Zhang, M.; Zheng, B.; Zhao, D.; Cheng, Y.; He, Z.; Su, M.; Xie, C.; Luo, M.; et al. Mitigating the Surface Reconstruction of Ni-Rich Cathode via P2-Type Mn-Rich Oxide Coating for Durable Lithium Ion Batteries. *ACS Appl. Mater. Interfaces* **2022**, *14*, 30398–30409. [CrossRef] [PubMed]
13. Li, X.; Gao, A.; Tang, Z.; Meng, F.; Shang, T.; Guo, S.; Ding, J.; Luo, Y.; Xiao, D.; Wang, X.; et al. Robust Surface Reconstruction Induced by Subsurface Ni/Li Antisites in Ni-Rich Cathodes. *Adv. Funct. Mater.* **2021**, *31*, 2010291. [CrossRef]
14. Xu, G.-L.; Liu, Q.; Lau, K.K.S.; Liu, Y.; Liu, X.; Gao, H.; Zhou, X.; Zhuang, M.; Ren, Y.; Li, J.; et al. Building ultraconformal protective layers on both secondary and primary particles of layered lithium transition metal oxide cathodes. *Nat. Energy* **2019**, *4*, 484–494. [CrossRef]
15. Yan, P.; Zheng, J.; Gu, M.; Xiao, J.; Zhang, J.-G.; Wang, C.-M. Intragranular cracking as a critical barrier for high-voltage usage of layer-structured cathode for lithium-ion batteries. *Nat. Commun.* **2017**, *8*, 14101. [CrossRef] [PubMed]
16. Kaufman, L.A.; Huang, T.-Y.; Lee, D.; McCloskey, B.D. Particle Surface Cracking Is Correlated with Gas Evolution in High-Ni Li-Ion Cathode Materials. *ACS Appl. Mater. Interfaces* **2022**, *14*, 39959–39964. [CrossRef]
17. Yan, P.; Zheng, J.; Liu, J.; Wang, B.; Cheng, X.; Zhang, Y.; Sun, X.; Wang, C.; Zhang, J.-G. Tailoring grain boundary structures and chemistry of Ni-rich layered cathodes for enhanced cycle stability of lithium-ion batteries. *Nat. Energy* **2018**, *3*, 600–605. [CrossRef]
18. Liu, Q.; Liu, Y.-T.; Zhao, C.; Weng, Q.-S.; Deng, J.; Hwang, I.; Jiang, Y.; Sun, C.; Li, T.; Xu, W.; et al. Conformal PEDOT Coating Enables Ultra-High-Voltage and High-Temperature Operation for Single-Crystal Ni-Rich Cathodes. *ACS Nano* **2022**, *16*, 14527–14538. [CrossRef]
19. Bi, Y.; Tao, J.; Wu, Y.; Li, L.; Xu, Y.; Hu, E.; Wu, B.; Hu, J.; Wang, C.; Zhang, J.-G.; et al. Reversible planar gliding and microcracking in a single-crystalline Ni-rich cathode. *Science* **2020**, *370*, 1313–1317. [CrossRef]
20. Song, B.; Li, W.; Oh, S.-M.; Manthiram, A. Long-Life Nickel-Rich Layered Oxide Cathodes with a Uniform Li_2ZrO_3 Surface Coating for Lithium-Ion Batteries. *ACS Appl. Mater. Interfaces* **2017**, *9*, 9718–9725. [CrossRef]
21. Hou, D.; Han, J.; Geng, C.; Xu, Z.; AlMarzooqi, M.M.; Zhang, J.; Yang, Z.; Min, J.; Xiao, X.; Borkiewicz, O.; et al. Surface coating by mechanofusion modulates bulk charging pathways and battery performance of Ni-rich layered cathodes. *Proc. Natl. Acad. Sci. USA* **2022**, *119*, e2212802119. [CrossRef]
22. Sungjemmenla, S.K.V.; Soni, C.B.; Kumar, V.; Seh, Z.W. Understanding the Cathode–Electrolyte Interphase in Lithium-Ion Batteries. *Energy Technol.* **2022**, *10*, 2200421. [CrossRef]
23. Liu, Y.-M.; Nicolau, B.G.; Esbenshade, J.L.; Gewirth, A.A. Characterization of the Cathode Electrolyte Interface in Lithium Ion Batteries by Desorption Electrospray Ionization Mass Spectrometry. *Anal. Chem.* **2016**, *88*, 7171–7177. [CrossRef] [PubMed]
24. Lin, R.; He, Y.; Wang, C.; Zou, P.; Hu, E.; Yang, X.-Q.; Xu, K.; Xin, H.L. Characterization of the structure and chemistry of the solid–electrolyte interface by cryo-EM leads to high-performance solid-state Li-metal batteries. *Nat. Nanotechnol.* **2022**, *17*, 768–776. [CrossRef] [PubMed]

25. Wheatcroft, L.; Klingner, N.; Heller, R.; Hlawacek, G.; Özkaya, D.; Cookson, J.; Inkson, B.J. Visualization and Chemical Characterization of the Cathode Electrolyte Interphase Using He-Ion Microscopy and In Situ Time-of-Flight Secondary Ion Mass Spectrometry. *ACS Appl. Energy Mater.* **2020**, *3*, 8822–8832. [CrossRef] [PubMed]
26. Bond, T.M.; Burns, J.C.; Stevens, D.A.; Dahn, H.M.; Dahn, J.R. Improving Precision and Accuracy in Coulombic Efficiency Measurements of Li-Ion Batteries. *J. Electrochem. Soc.* **2013**, *160*, A521. [CrossRef]
27. Hall, D.S.; Gauthier, R.; Eldesoky, A.; Murray, V.S.; Dahn, J.R. New chemical insights into the beneficial role of Al_2O_3 cathode coatings in lithium-ion cells. *ACS Appl. Mater. Interfaces* **2019**, *11*, 14095–14100. [CrossRef]
28. Ma, T.; Xu, G.-L.; Li, Y.; Wang, L.; He, X.; Zheng, J.; Liu, J.; Engelhard, M.H.; Zapol, P.; Curtiss, L.A.; et al. Revisiting the Corrosion of the Aluminum Current Collector in Lithium-Ion Batteries. *J. Phys. Chem. Lett.* **2017**, *8*, 1072–1077. [CrossRef]
29. Xie, Y.; Gao, H.; Gim, J.; Ngo, A.T.; Ma, Z.-F.; Chen, Z. Identifying Active Sites for Parasitic Reactions at the Cathode–Electrolyte Interface. *J. Phys. Chem. Lett.* **2019**, *10*, 589–594. [CrossRef]
30. Zeng, X.; Xu, G.-L.; Li, Y.; Luo, X.; Maglia, F.; Bauer, C.; Lux, S.F.; Paschos, O.; Kim, S.-J.; Lamp, P.; et al. Kinetic Study of Parasitic Reactions in Lithium-Ion Batteries: A Case Study on $LiNi_{0.6}Mn_{0.2}Co_{0.2}O_2$. *ACS Appl. Mater. Interfaces* **2016**, *8*, 3446–3451. [CrossRef]
31. Chen, Z. Chasing protons in lithium-ion batteries. *Chem. Commun.* **2022**, *58*, 10127–10135. [CrossRef]
32. Cai, J.; Yang, Z.; Zhou, X.; Wang, B.; Suzana, A.; Bai, J.; Liao, C.; Liu, Y.; Chen, Y.; Song, S.; et al. Unveiling the parasitic-reaction-driven surface reconstruction in Ni-rich cathode and the electrochemical role of Li_2CO_3. *J. Energy Chem.* **2023**, *85*, 126–136. [CrossRef]
33. Renfrew, S.E.; McCloskey, B.D. Residual Lithium Carbonate Predominantly Accounts for First Cycle CO_2 and CO Outgassing of Li-Stoichiometric and Li-Rich Layered Transition-Metal Oxides. *J. Am. Chem. Soc.* **2017**, *139*, 17853–17860. [CrossRef]
34. Renfrew, S.E.; McCloskey, B.D. Quantification of surface oxygen depletion and solid carbonate evolution on the first cycle of $LiNi_{0.6}Mn_{0.2}Co_{0.2}O_2$ electrodes. *ACS Appl. Energy Mater.* **2019**, *2*, 3762–3772. [CrossRef]
35. Sattar, T.; Sim, S.-J.; Jin, B.-S.; Kim, H.-S. Dual function Li-reactive coating from residual lithium on Ni-rich NCM cathode material for Lithium-ion batteries. *Sci. Rep.* **2021**, *11*, 18590. [CrossRef] [PubMed]
36. Liu, D.; Thomas, T.; Gong, H.; Li, F.; Li, Q.; Song, L.; Azhagan, T.; Jiang, H.; Yang, M. A mechanism of alkali metal carbonates catalysing the synthesis of β-hydroxyethyl sulfide with mercaptan and ethylene carbonate. *Org. Biomol. Chem.* **2019**, *17*, 9367–9374. [CrossRef] [PubMed]
37. Huang, S.; Liu, S.; Li, J.; Zhao, N.; Wei, W.; Sun, Y. Effective synthesis of propylene carbonate from propylene glycol and carbon dioxide by alkali carbonates. *Catal. Lett.* **2006**, *112*, 187–191. [CrossRef]